


# Mechanical enhancement of natural-curing geopolymer via shear-exfoliation graphene addition for sustainable paving blocks

Amun Amri<sup>1\*</sup>, Rahmat Zega<sup>1</sup>, Namira Herliana Putri<sup>1</sup>, Dhina Febryza<sup>1</sup>,  
Desi Heltina<sup>1</sup>, Azhari<sup>2</sup>, Bambang Sujatmoko<sup>2</sup>, Fri Murdiya<sup>3</sup>

<sup>1</sup> Department of Chemical Engineering, University of Riau, Panam, Pekanbaru 28293, Indonesia

<sup>2</sup> Department of Civil Engineering, University of Riau, Panam, Pekanbaru 28293, Indonesia

<sup>3</sup> Department of Electrical Engineering, University of Riau, Panam, Pekanbaru 28293, Indonesia

\* Corresponding author's e-mail: amun.amri@eng.unri.ac.id

## ABSTRACT

The compressive strength and surface hardness of fly-ash based geopolymer paving block composites (GPBC), fabricated in a room temperature curing process (natural curing), have been successfully improved with the addition of low-cost liquid shear-exfoliation graphene (LSE-G) additives. The incorporation of LSE-G represents a breakthrough enabling natural-curing geopolymer composites to compete with conventional geopolymer materials while being easier and more economical to produce, making them suitable for small-scale production by local communities. Natural-curing GPBC was synthesized by mixing coal fly ash, sand,  $\text{Na}_2\text{SiO}_3$ , NaOH, and LSE-G solution with concentrations of 20 mg/ml, 40 mg/ml, and 80 mg/ml. The GPBC were characterized using compressive strength tests, Vickers hardness, water absorption tests, Raman spectroscopy (RS), scanning electron microscopy-EDX Spectrum (SEM-EDX), and transmission electron microscopy (TEM). Raman spectroscopy analysis indicated that LSE-G was well-distributed within the geopolymer matrix. The addition of LSE-G up to a concentration of 40 mg/ml increased compressive strength of geopolymer composite to 21.83 MPa (a 23.4% increase) and surface hardness to 122.5 Hv (a 6.15% increase). However, higher concentrations led to a decline in both parameters. SEM analysis revealed a denser and more compact geopolymer composite structure when LSE-G was added, with a reduction in porosity by 26.80%, which also resulted in a decrease in water absorption by 10.71%. EDX analysis supported the RS results, showing that LSE-G was homogeneously incorporated into the composite matrix. TEM analysis explained that adding LSE-G up to a certain limit could enhance the density and compactness of the material. LSE-G has proven to be an effective and promising additive for improving the mechanical properties of natural-curing geopolymer paving block composites.

**Keywords:** geopolymer paving block composite, low-cost few-layer graphene, compressive strength properties, surface hardness, morphology.

## INTRODUCTION

Geopolymer is an environmentally friendly alternative material compared to Portland cement, as it can reduce carbon emissions by up to 90% (Amran et al., 2020; Salman et al., 2023). Additionally, geopolymer offers several advantages, such as high early strength, excellent durability, thermal stability, and low shrinkage (Do et al., 2020; Zerfu and Ekaputri, 2016). Geopolymer is a cost-effective alternative material that has been widely applied in various fields, such as

concrete production, sealants, ceramics, and paving blocks (Guo et al., 2022). The development of fly ash-based geopolymer paving blocks represents a promising utilization alternative, considering the abundant supply of fly ash as waste from power plants (PLTU) or other industrial by-products (Jelic et al., 2023).

The curing process, which involves heat treatment (at temperatures of 60–80 °C) for 24 hours, presents one of the challenges in geopolymer material development due to its high energy costs and significant investment requirements (Kavipriya,

2022). Therefore, the development of a natural-curing method (natural curing at ambient temperature or environment) has become an attractive alternative (Zhang et al., 2021). However, the use of natural curing methods may result in lower strength for the geopolymer compared to conventional curing processes. To address this issue, graphene, as a 2D nanomaterial, offers a promising solution due to its exceptional light weight and remarkable strength and flexibility properties. Thus, graphene is expected to enhance the mechanical properties of geopolymers, particularly in improving compressive strength (Abiodun et al., 2023).

Chu et al. (2020) conducted a study to investigate the effect of adding graphene oxide at varying concentrations (0.025–0.075%) on the mechanical properties and durability of ultra-high-performance concrete (UHPC) made from recycled sand. The addition of graphene oxide resulted in a reduction in porosity by 4.45–11.35%, while compressive strength, flexural strength, tensile strength, and elastic modulus increased by 8.24–16.83%, 11.26–26.62%, 15.63–29.54%, and 5.84–12.25%, respectively. However, the inclusion of cement and steel fibers increased production costs, making it less suitable for large-scale production (Chu et al., 2020). Abiodun et al. (2023) studied the effects of adding pristine graphene at varying concentrations (0.05–0.3 wt.%) on the mechanical properties of geopolymer mortar. The addition of 0.07 wt.% pristine graphene increased compressive strength, tensile strength, and flexural strength by 14.4%, 25.96%, and 17.35%, respectively. However, the curing process for geopolymer using pristine graphene is challenging to implement in large-scale paving block production and incurs high production costs (Abiodun et al., 2023). Ranjbar et al. (2015) reported that the addition of graphene nanoplatelets (GNPs) could enhance the compressive and flexural strength of fly ash-based geopolymers by 2.16 times compared to non-graphene geopolymers. However, the synthesis process for GNPs using the Hummers method makes it uneconomical as an additive for geopolymer paving blocks.

Amri et al. (2020) successfully synthesized fly ash-based geopolymer mortar with NaOH activator and low-cost few-layer graphene (LSE-G) as a reinforcing material. LSE-G was produced using a simple turbulence-assisted shear exfoliation (TASE) method with a kitchen blender. The compressive strength, porosity, and water absorption values of the synthesized geopolymer were

29.544 MPa, 10.903%, and 6.034%, respectively. However, the curing process in a heating oven proved to be less feasible due to the high energy costs and the significant investment required, which hinders the diffusion of this technology within the community (Amri et al., 2020).

This study aims to develop fly ash-based geopolymer paving blocks with a natural-curing system, incorporating low-cost few-layer graphene (LSE-G) as an additive. The effects of adding LSE-G on compressive strength, surface hardness, water absorption, morphology, and the homogeneity of graphene distribution were investigated. The main findings of this study show that the addition of LSE-G to the geopolymer composite increased compressive strength by up to 23.4% and surface hardness by up to 6.15% compared to the geopolymer without graphene, with LSE-G being well-distributed within the composite. The use of LSE-G as a substitute for the curing process in a heating oven is considered more advantageous due to the low-cost and environmentally friendly production of graphene despite a slightly lower compressive strength compared to conventional geopolymers. Therefore, the use of LSE-G as an additive for producing geopolymer paving blocks in a natural curing system holds promising prospects.

## MATERIALS AND METHODS

### Preparation of graphene

Graphene was synthesized from pure graphite using the turbulence-assisted shear exfoliation method in a simple and environmentally friendly rotating-blade mixer (kitchen blender) (Varrla et al., 2014). After the exfoliation process was completed, the solution was left for 24 hours, and the sediment was removed. The graphene solution was then placed in an oven at 60 °C to reduce the water content, resulting in graphene concentrations of 20 mg/ml, 40 mg/ml, and 80 mg/ml.

### Preparation of geopolymer paving block composite

The geopolymer paving block composite was synthesized by mixing 85% solid materials and 15% liquid materials into a dough mixer. The composition of the solid materials used was coal fly ash: casting sand: medium sand in a ratio of 25%: 62.5%: 12.5%. The liquid materials

consisted of  $\text{Na}_2\text{SiO}_3$ :  $\text{NaOH}$  10 M in a ratio of approximately 2.5:1, along with a graphene solution with varying concentrations of 20–80 mg/ml. The mixed materials were then placed into metal molds and pressed using a hydraulic press. The molded geopolymer composite was left for natural curing at room temperature for 28 days.

## Characterization

The geopolymer composite was characterized through mechanical property analysis, which included compressive strength, water absorption, and Vickers hardness testing. The compressive strength analysis followed the ASTM standard (2012) and was calculated using Equation 1.

$$f_{c'} = \frac{P}{A} \quad (1)$$

where: compressive strength ( $\text{MPa}$ ) is denoted as  $f_{c'}$ ,  $P$  is the maximum load ( $\text{N}$ ), and  $A$  is the surface area under load ( $\text{mm}^2$ ). Water absorption testing followed the ASTM standard (2006) and was calculated using Equation 2.

$$\text{Water absorption (\%)} = \frac{A-B}{B} \times 100\% \quad (2)$$

where:  $A$  is the weight of the water-saturated geopolymer composite after immersion ( $\text{kg}$ ), and  $B$  is the dry weight of the specimen ( $\text{kg}$ ).

Raman spectroscopy analysis was performed using a WITec Alpha 300R Raman spectrometer.

Molecular vibrations were excited using a 532 nm wavelength. Morphological analysis included scanning electron microscopy-EDX spectrum (SEM-EDX) using an SEM SU 3500 instrument and transmission electron microscopy (TEM) with an HR TEM H9500 instrument. Surface hardness testing was conducted at 3 test points using a micro-Vickers hardness testing machine with a load of 0.3 N for 10 seconds.

## RESULT AND DISCUSSION

### Raman spectroscopy analysis

Figure 1 shows the Raman spectra of the geopolymer paving block composite samples containing 2.75% graphene with varying concentrations (0–80 mg/ml). From Figure 1, it can be observed that the geopolymer paving blocks with the addition of graphene at concentrations of 40 mg/ml and 80 mg/ml exhibit dynamic and fluctuating spectral patterns with several spectral peaks, compared to the smooth spectrum of the geopolymer without graphene addition. Characteristic graphene peaks in the composite paving block are observed around  $\sim 1333.88 \text{ cm}^{-1}$ ,  $\sim 1609.65 \text{ cm}^{-1}$ , and  $\sim 2774 \text{ cm}^{-1}$  (2D band), which correspond to the D band, G band, and 2D band, respectively. The presence of these peaks indicates that graphene has been well-distributed within the paving block composite structure. Meanwhile, graphite exhibits three characteristic peaks: the G band ( $1584.20 \text{ cm}^{-1}$ ) and the 2D band ( $2718.19 \text{ cm}^{-1}$ ),

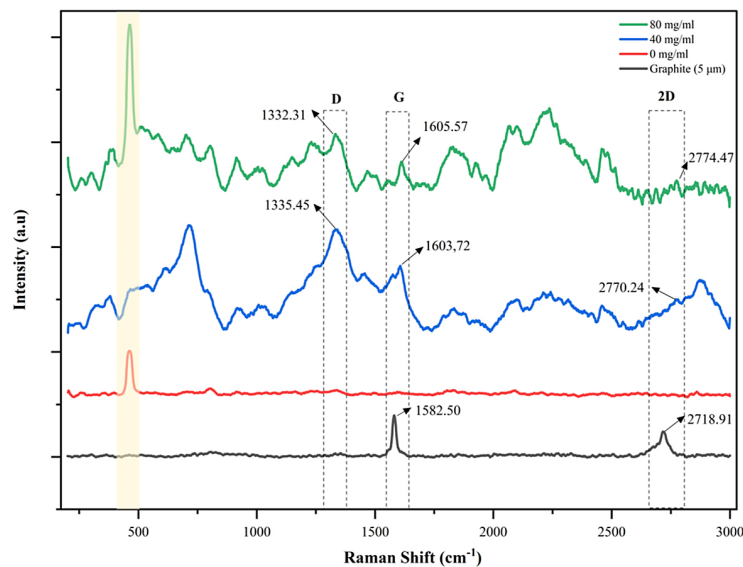


**Figure 1.** Raman spectra of geopolymer with varying graphene concentrations: 0 mg/ml, 40 mg/ml, 80 mg/ml

without the D band peak. These peaks are considered the fingerprint of graphite material (Zhang et al., 2018). The absence of the D band peak indicates that the graphite precursor used is free from defects or contains very low defects.

In Figure 1, a shift in the D peak in the geopolymer composite is observed, indicating a change in the crystal structure of graphene. This shift is due to interactions with the geopolymer matrix, which can affect the distribution of defects in the material. A study by (Kaftelen-Odabaşı, 2024) explains that electron-phonon interactions and defects in the graphene structure cause the D peak shift. The D peak appears in defect or edge regions, altering the phonon energy and electron-phonon interactions. Research by (Ni et al., 2008) elaborates that the G peak can shift when foreign atoms or molecules, referred to as doping, are added, leading to the removal of the nonadiabatic anomaly at the Kohn point in the  $\Gamma$  zone. Similarly, (Zhong et al., 2013) reported that the shift in the G peak is caused by the removal of the nonadiabatic Kohn anomaly in graphene due to electrochemical doping. The Kohn anomaly refers to the reduction in the  $E_{2g}$  phonon vibration frequency induced by electron-phonon coupling (EPC). Electrochemical doping removes the Kohn anomaly, increasing the  $E_{2g}$  phonon vibration frequency.

According to (Ni et al., 2008), the 2D peak can shift due to hole doping and electron doping, which can modify the equilibrium lattice parameters induced by charge transfer. The 2D peak is not significantly observed around  $2774\text{ cm}^{-1}$  because the 2D peak of multilayer graphene appears broader and less intense (Papanai et al., 2020). Furthermore, the graphene peak becomes broader and shifts when the thickness of the graphene increases. Research by (Eckmann et al., 2013) also mentions that the position of the 2D peak can shift with an increase in defect concentration. The uneven distribution of graphene in the composite leads to variations in the Raman spectrum, indicating areas with different layer counts and defect densities (No et al., 2018).

In Figure 1, additional peaks are observed around  $465\text{ cm}^{-1}$ ,  $716\text{ cm}^{-1}$ ,  $1800\text{ cm}^{-1}$ ,  $2240\text{ cm}^{-1}$ , and  $2460\text{ cm}^{-1}$ . According to (Kosor et al., 2016), the peak around  $465\text{ cm}^{-1}$  is caused by the intra-tetrahedral vibration of the  $\text{SiO}_4$  tetrahedra, which polymerizes during the geopolymerization reaction, as indicated by the peak around  $460\text{ cm}^{-1}$ . Additionally, the peak around  $716\text{ cm}^{-1}$  is attributed to the asymmetric bending mode of

$\text{CO}_3$  (carbonate), as indicated by the peak around  $713\text{ cm}^{-1}$ . The peak around  $1800\text{ cm}^{-1}$  is caused by the combination of acoustic transverse phonons in-plane (iTA) and longitudinal optical phonons (LO) (Rao et al., 2011). The intensity of this peak decreases as the number of layers increases, and it is not visible in graphite (Rao et al., 2011). The peak around  $2240\text{ cm}^{-1}$  is tentatively assigned to the combination of in-plane optical transverse phonon mode (iTO) and TA phonon ( $\sigma\text{TO}+\text{LO}$ ) near the K point in the graphene Brillouin zone (Rao et al., 2011). According to (Rao et al., 2011), the frequency of the peak around  $2220\text{ cm}^{-1}$  decreases linearly with increasing graphene layers. Another peak at a Raman shift of  $2460\text{ cm}^{-1}$  is a D+D1 peak found in graphene nanoplatelets, representing the overtone (multiples of the fundamental frequency) of the D peak (Dovbeshko et al., 2014). A peak also appears around  $2880\text{ cm}^{-1}$  in the geopolymer composite with a graphene concentration of  $40\text{ mg/ml}$ , related to the presence of the G' peak (Hu et al., 2014). Meanwhile, the composite with a graphene concentration of  $80\text{ mg/ml}$  does not exhibit this peak, possibly due to the aggregation of graphene in the composite. At higher concentrations, graphene shows changes in its structural and vibrational properties due to increased density and potential structural defects. These changes can significantly affect the vibrational modes of graphene, such as those related to the overtone ( $2880\text{ cm}^{-1}$ ), which become weaker or even disappear (Dabhi and Jha, 2017).

### Compressive strength analysis

Figure 2 shows the effect of varying graphene concentrations on the compressive strength of geopolymer paving block composites with concentrations of  $0\text{--}80\text{ mg/ml}$ . From Figure 2, it can be seen that the addition of  $20\text{--}40\text{ mg/ml}$  of graphene significantly increases the compressive strength of the geopolymer composite, especially at the  $40\text{ mg/ml}$  concentration, which demonstrates the best performance with a 23.39% increase in compressive strength compared to the geopolymer without graphene. However, at a higher graphene concentration of  $80\text{ mg/ml}$ , the compressive strength decreases by approximately 3.2%. The increase in compressive strength with the higher graphene content is attributed to the good dispersion of graphene within the geopolymer composite, which fills the pores of the matrix, resulting in a denser and stronger structure (Amri



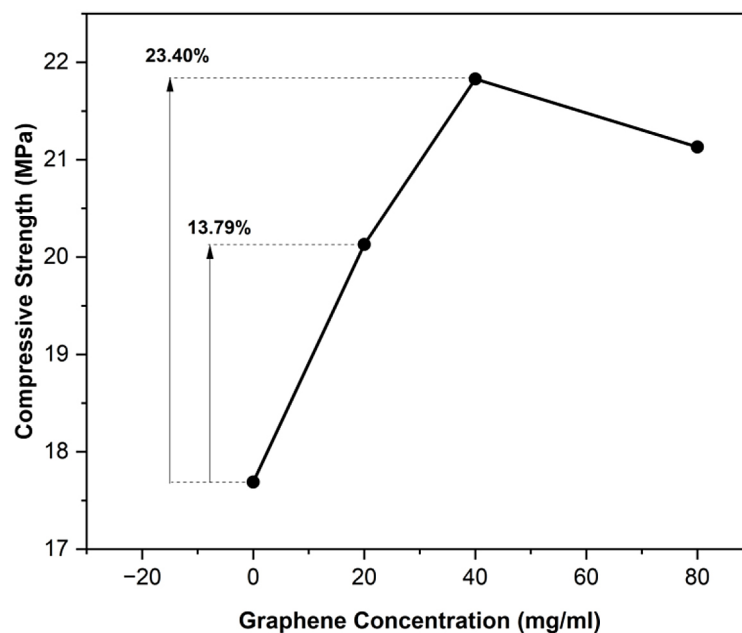


**Figure 2.** Effect of graphene concentration on the compressive strength of geopolymer composite after 28 days

et al., 2019). The addition of graphene can alter the microstructure, making it more compact and reducing internal voids (Zhang and Lu, 2018).

The presence of graphene also accelerates the geopolymerization process and the hydration rate, thereby promoting nucleation and crystallization within the geopolymer gel, which strengthens the material (Fan et al., 2023). The high strength of graphene also aids in better stress distribution within the geopolymer matrix, reducing the likelihood of crack propagation and improving the overall toughness of the composite (Ranjbar et al., 2015). The enhancement of mechanical properties in graphene-added geopolymer composites has been reported by (Singh, 2018), who noted that graphene acts as a protective or reinforcing layer, wrapping and strengthening the composite structure. However, the compressive strength obtained in this study is still lower than that of geopolymer produced conventionally through curing processes, which generally have compressive

strengths ranging from ~37.24 MPa (moist curing) (Chairunnisa et al., 2024) and 22.34–41 MPa (heat curing) (Table 1) (Ahmad and Rashid, 2022; Amri et al., 2020; Bai et al., 2022; Merino-Lechuga et al., 2024; Sukmak et al., 2013). This is because, in moist curing, moisture retention is ensured during the drying process, which is crucial for the chemical reaction between the alkaline activator and aluminosilicate materials in developing the high-strength three-dimensional cross-linked bond network in geopolymers. This method also prevents microcracks caused by dehydration (Lee et al., 2016). Meanwhile, in heat curing, heat can increase the reaction rate, thereby accelerating the geopolymerization process (Wang et al., 2012). This is due to the enhanced dissolution of aluminosilicate materials at high temperatures, which promotes the formation of C–(A)–S–H gel, geopolymer gel, and calcium chloroaluminate hydrate, which fill the pores and increase the compactness of the structure (Bai et al., 2022).

**Table 1.** Compressive strength data of geopolymers based on curing method and curing time

Researcher	Curing method	Curing time (h)	Compressive strength (MPa)
(Merino-Lechuga et al., 2024)	Heat curing (70 °C)	1–7	27.40–31.10
(Chairunnisa et al., 2024)	Moist curing	14–28	35.03–37.68
(Bai et al., 2022)	Heat curing (90 °C)	3–28	22.98–27.91
(Ahmad & Rashid, 2022)	Heat Curing (60–110 °C)	7	22–34
(Amri et al., 2020)	Heat Curing (80 °C)	28	29.54
(Sukmak et al., 2013)	Heat Curing (60–85 °C)	7–28	32–41

The decrease in the compressive strength of the geopolymer paving block composite at the graphene concentration of 80 mg/ml is due to the tendency of graphene to agglomerate at high concentrations, which reduces the uniform distribution and weakens the material (Abiodun et al., 2023). Several researchers have shown that the compressive strength of geopolymer composites increases with the addition of graphene up to an optimal point and then decreases at higher graphene concentrations (Zhang and Lu, 2018). Researchers (Danial et al., 2019; Shamsaei et al., 2018) also reported that excess graphene addition can reduce the mechanical properties of the geopolymer, as at high concentrations, graphene sheets tend to agglomerate easily. The large surface area and Van der Waals force interactions cause the graphene sheets to stack and lead to agglomeration, negatively impacting the microstructure and mechanical properties of the composite (Ranjbar et al., 2015). This can hinder the uniform distribution and effectiveness of graphene within the geopolymer composite matrix (Ranjbar et al., 2015).

Based on Figure 2, it can be observed that the compressive strength of the synthesized paving block composite has met the criteria of SNI 03-0691-1996 for medium-strength concrete bricks (B), which range from 20–35 MPa and are used for park equipment. However, this value is still lower compared to the minimum value of 55 MPa, as specified by ASTM C936 and ASTM C1272 for type R paving blocks (Pandey et al., 2024). The increase in the strength of geopolymer composites typically follows a symmetric curve pattern as the

graphene concentration increases. This means that at a certain point, the addition of graphene results in a significant increase in compressive strength, but beyond the optimal point, the compressive strength may decrease due to factors such as graphene aggregation and interactions with the composite mixture. As reported by (Dalal and Dalal, 2021), nano concrete composites with the addition of 1 mg/l of graphene can improve compressive strength by 27%, but adding more than 1 mg/l leads to a decrease in compressive strength performance (Dalal and Dalal, 2021).

### Water absorption analysis

Figure 3 shows the water absorption values of geopolymer paving block composites with varying graphene concentrations of 0–80 mg/ml. Water absorption generally has a detrimental effect on the mechanical properties of geopolymer composites. Increased water absorption can lead to a reduction in compressive strength due to the weakening of the geopolymer matrix and the formation of voids and cracks (Guerrieri et al., 2020). From Figure 3, it can be observed that water absorption decreases as the graphene concentration in the geopolymer composite increases. The lowest water absorption value is shown at the 40 mg/ml graphene concentration, which is 5.25%, with a reduction of about 10.71%. In contrast, the highest water absorption value is seen in the geopolymer composite without graphene addition (0 mg/ml), at 5.88%. According to (Susanto et al., 2024), the addition of graphene into fly ash-based geopolymer composites

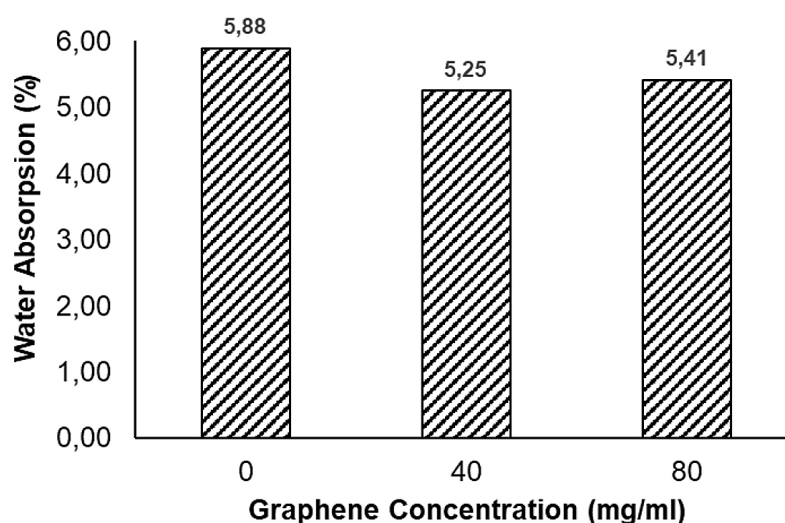


**Figure 3.** Effect of graphene concentration on water absorption values in geopolymer paving block composites

reduces the total porosity, the total number of pores, and their distribution due to the densification of the specimen's bulk matrix. As a result, water absorption decreases, the specimen's density increases, and consequently, mechanical properties such as compressive strength also improve (Susanto et al., 2024).

However, as seen in Figure 3, the water absorption value at a concentration of 80 mg/ml shows a slight increase. This may be due to the agglomeration of graphene, which results in less homogeneous distribution, leading to higher porosity in the composite. This, in turn, increases water absorption and reduces material density (Susanto et al., 2024). A higher water absorption value indicates a higher pore volume in the paving block (Jonbi and Fulazzaky, 2020). Research by (Uma Magesvari et al., 2020) shows that the void ratio is directly proportional to permeability. As the voids or porosity in the geopolymer mix increases, the material's ability to absorb and transmit water also increases. According to SNI 03-0361-1996, the water absorption test results for geopolymer paving blocks with 0–80 mg/ml concentrations fall into the B quality category. B-grade paving blocks, with an average maximum water absorption of 6%, can be used for parking lot pavements. This value meets the requirements of ASTM C1272, which specifies water absorption of less than 6% (Pandey et al., 2024).

### Vickers hardness analysis

Table 2 shows the Vickers hardness values of geopolymer paving block composites containing 2.75% graphene with varying concentrations of

0–80 mg/ml. From Table 1, it can be observed that the Vickers hardness of geopolymer paving blocks without graphene addition remains relatively constant. In contrast, the composites with graphene addition show more fluctuating hardness values, which are related to the level of homogeneity of the composite. There is a linear relationship between Vickers hardness and compressive strength in geopolymers. Higher Vickers hardness generally indicates higher compressive strength (Subaer et al., 2017). From Table 1, it is evident that the highest hardness value is observed at the 40 mg/ml graphene concentration, which is 122.5 Hv, representing a 6.15% increase. However, this value decreases by approximately 0.33% when the graphene concentration is increased to 80 mg/ml. These results are higher than those reported by (Zainal et al., 2016), which indicated a maximum Vickers hardness of 118.6 Hv for geopolymer with a heat curing system using an oven at 60 °C. Meanwhile, the lowest hardness was obtained for the geopolymer composite without graphene addition (0 mg/ml), which was 115.4 Hv.

The addition of graphene to geopolymer composites has been observed to increase Vickers hardness due to the refinement and enhancement of the microstructure (Benjamin et al., 2023). According to (Jonbi and Fulazzaky, 2020), the increase in Vickers hardness of geopolymer paving block composites correlates positively with the increase in compressive strength. They mentioned that by optimizing the activator composition ratio, both the hardness and compressive strength of the geopolymer would increase. The addition of graphene can improve compressive strength due to its exceptional strength and good distribution

**Table 2.** Vickers hardness values in geopolymer paving block composites

Concentration (mg/ml)	Test point	Diagonal		Hardness (Hv)	Average (Hv)
		D1 (X)	D2 (Y)		
0	1	66.61	72.22	115.5	115.4
	2	68.33	72.99	111.4	
	3	67.53	68.96	119.4	
40	1	67.50	63.83	129.0	122.5
	2	66.22	67.38	124.7	
	3	69.23	70.67	113.7	
80	1	67.84	68.36	120.0	122.1
	2	65.15	66.84	127.7	
	3	69.09	67.92	118.5	

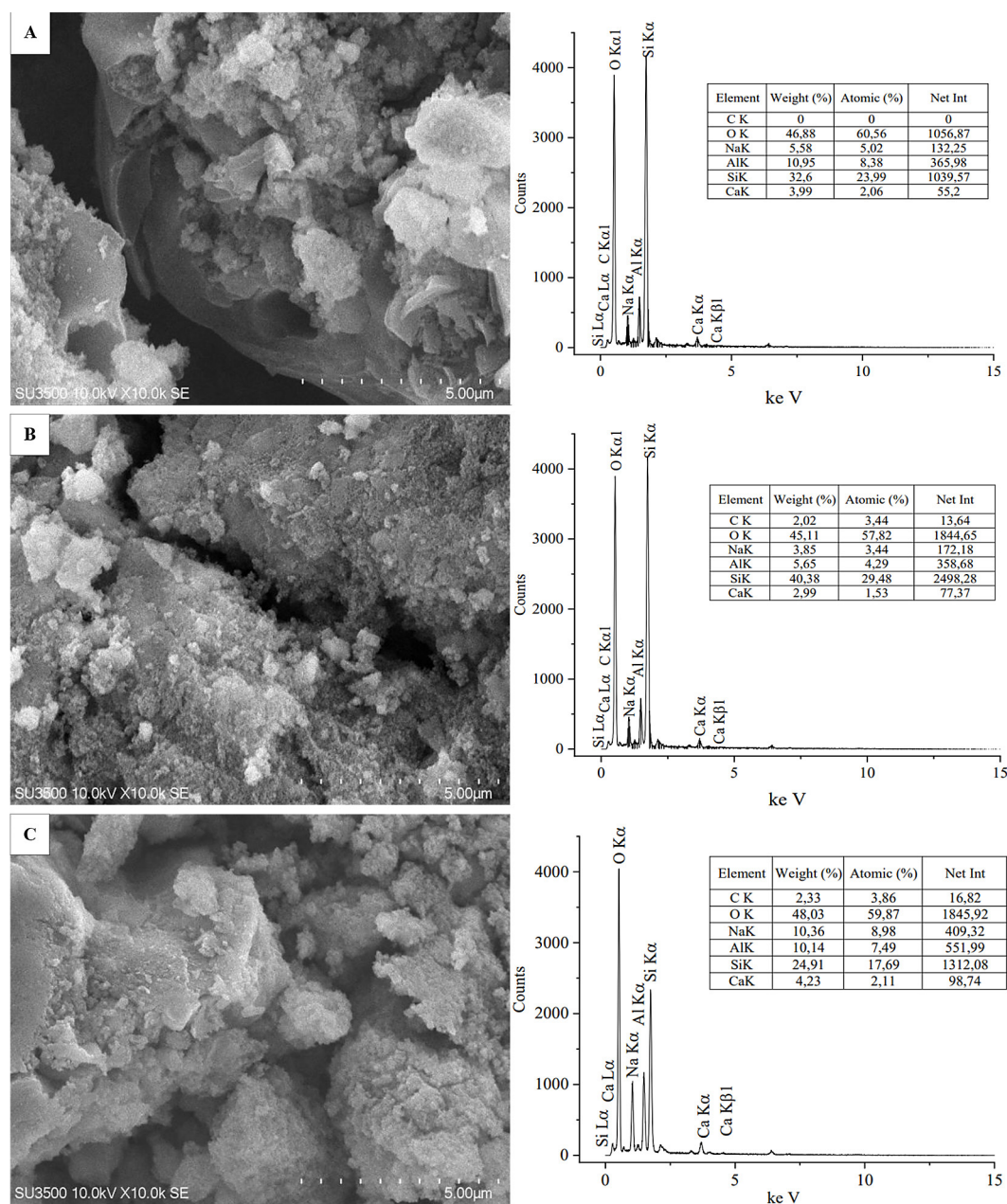
**Note:** D1 (X) and D2 (Y) represent the diagonal length of the indentation test. Hv is the hardness value of each test point.

within the geopolymer paving block composite (Yan et al., 2016). Furthermore, according to studies by (Danial et al., 2019; Shamsaei et al., 2018), graphene is capable of filling pores and cavities, which strengthens the geopolymer. The decrease in compressive strength at the graphene concentration of 80 mg/ml is due to the excessive addition of graphene, which can lead to agglomeration. The agglomeration of graphene in the geopolymer composite results in suboptimal dispersion of graphene particles and creates voids within the composite (Shamsaei et al., 2018). The fluctuating Vickers hardness indicates the

inhomogeneous distribution of graphene in the geopolymer composite. Therefore, it is necessary to optimize the amount of graphene added to the geopolymer composite.

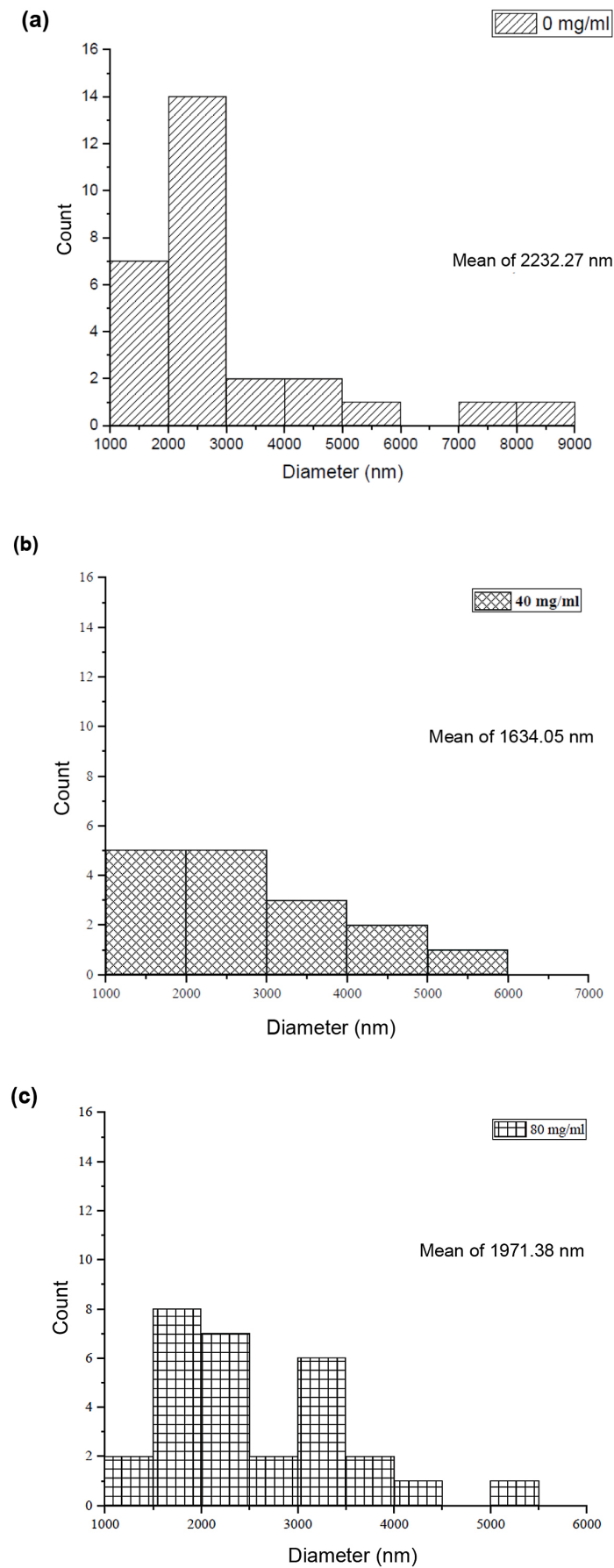
### Scanning electron microscopy-EDX spectrum (SEM-EDX) analysis

Figure 4 displays the morphology and micro-components of the geopolymer paving block composite investigated using SEM-EDX. In Figure 4a, the surface of the geopolymer composite without graphene addition shows a relatively



**Figure 4.** SEM-EDX analysis of geopolymer paving block composite at graphene concentrations (a) 0 mg/ml, (b) 40 mg/ml, (c) 80 mg/ml





**Figure 5.** Porosity distribution in geopolymer paving block composites with varying graphene concentrations: (a) 0 mg/ml; (b) 40 mg/ml; (c) 80 mg/ml

rough and porous texture. The constituent particles of the geopolymer composite appear loosely bound, resulting in a more open structure. In Figs. 4b and 4c, the addition of graphene leads to a more compact and denser structure in the geopolymer composite compared to the one without graphene. This is due to the ability of nano-graphene technology to fill the voids in the geopolymer composite (Amri et al., 2018). The two-dimensional structure of graphene, with its high surface area and strong interfacial interactions with the matrix material, serves as a template to form a binding network within the composite matrix (Cremonezzi et al., 2023). The formation of secondary bonds between carbon atoms on the graphene surface and oxygen, sodium, and silicon atoms in the geopolymer matrix helps improve the mechanical properties of the composite (Amri et al., 2023). A similar finding was reported by (Bellum et al., 2020), where the addition of graphene at the optimum concentration significantly altered the microstructure of the geopolymer composite, enhancing its mechanical properties, reducing porosity, and increasing compactness. The surface of the geopolymer paving block composite with 80 mg/ml graphene addition shows morphology and porosity similar to that of the composite with 40 mg/ml but with a denser and more compact appearance (Figure 4c).

The presence of graphene is difficult to observe and distinguish directly through SEM images (Figure 4) due to its thin nature and lateral size being at the nano/sub-micro scale (below the detection limit of SEM). Additionally, the amount of graphene added to the composite is relatively small (2.75%). However, based on the EDX analysis results, it is evident that the addition of graphene at concentrations of 40 mg/ml and 80 mg/ml increases the carbon (C) content in the geopolymer composite sample compared to the sample without graphene, which has a carbon content of 0%. EDX analysis in Figure 4a shows that the geopolymer composite without graphene addition exhibits the primary components of Oxygen (O) and Silicon (Si) with high intensity. Other components, such as Sodium (Na) and Aluminum (Al), are also detected in smaller amounts. Meanwhile, in Figs. 4b and 4c, the geopolymer composites with 40 mg/ml and 80 mg/ml graphene addition show the presence of carbon (C), indicating that graphene has been homogenized within the geopolymer paving block composite. The pore size distribution analysis was further conducted using

*ImageJ software*. From Figure 5a, it can be observed that there is a decrease in porosity in the geopolymer composite with the addition of 40 mg/ml graphene by 26.80% compared to the geopolymer without graphene. A study by (Chintalapudi and Pannem, 2020) reported that the addition of graphene can fill micropores, thus reducing the porosity in the composite. However, further addition of graphene at 80 mg/ml leads to a slight increase in porosity, around 17.11%, compared to the composite with 40 mg/ml graphene. This is suspected to be due to graphene agglomeration within the composite. Although graphene is relatively homogeneously distributed in the geopolymer matrix, the possibility of overlapping and agglomeration still exists (Ranjbar et al., 2015). A study by (Shamsaei et al., 2018) reported that graphene agglomeration can create small voids, which can increase the porosity in the composite.

#### Transmission electron microscopy (TEM) analysis

Figure 6 shows the TEM analysis of geopolymer paving block composites with varying graphene concentrations of 0 mg/ml, 40 mg/ml, and 80 mg/ml. In Figure 6a, it can be seen that the geopolymer paving block composite without graphene addition (0 mg/ml) displays a porous structure, which reduces the material density and affects its mechanical properties, making the geopolymer more prone to damage and cracking (Fiset et al., 2020). In Figs. 6b and 6c, it is clear that the geopolymer paving blocks with 40 mg/ml and 80 mg/ml graphene addition are more compact compared to the ones without graphene. In this case, graphene acts as a network template that links the different sections within the geopolymer composite (Cremonezzi et al., 2023).

In Figure 6b, no porous structure is observed on the surface of the geopolymer composite, as seen in Figure 6a, indicating that graphene has been homogeneously distributed and filled the empty spaces in the composite matrix. Graphene not only fills the pores in the geopolymer but also acts as a binding agent, enhancing the cohesion and mechanical properties of the material (Zhang et al., 2020). Graphene can chemically bond with the geopolymer matrix through a common condensation reaction, resulting in a denser interfacial region. These interfacial bonds strengthen the structure and help prevent crack formation (Zhang et al., 2020). Meanwhile, as

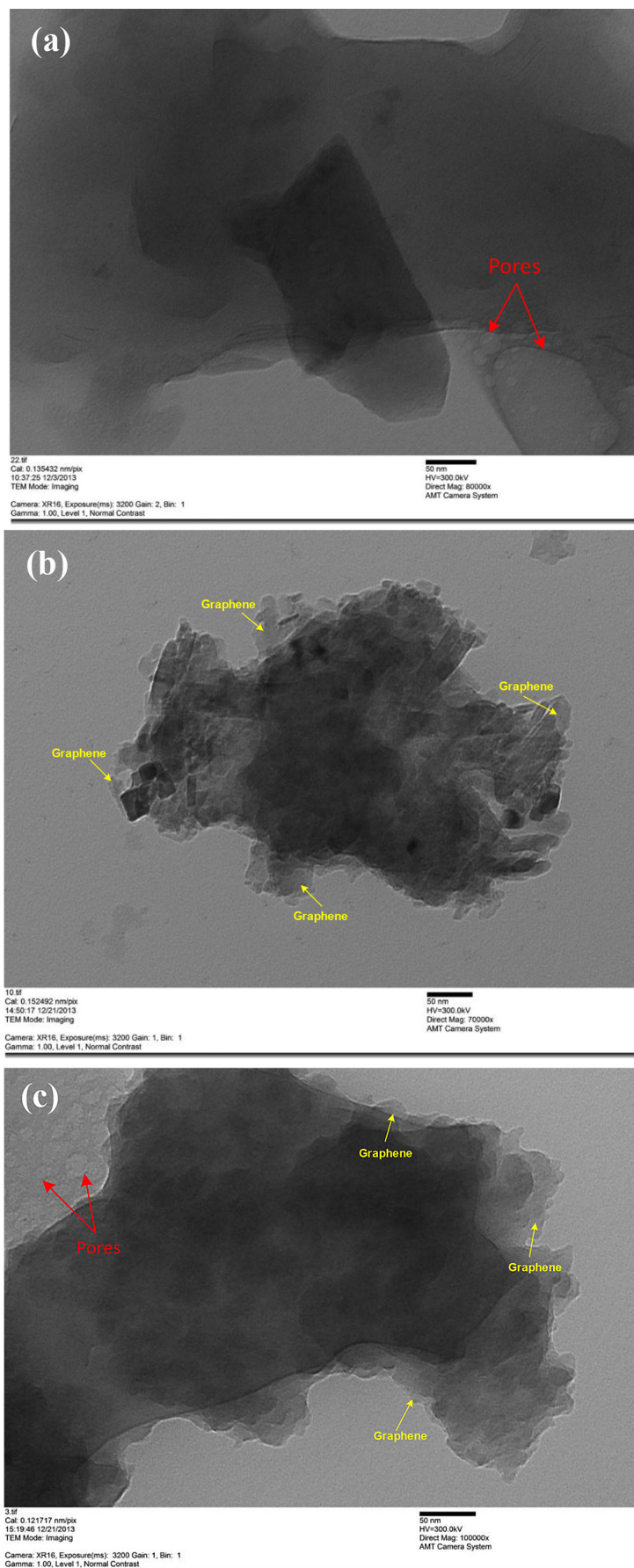


**Figure 6.** TEM analysis of geopolymer paving block composites with varying graphene concentrations: (a) graphene 0 mg/ml; (b) graphene 40 mg/ml; (c) graphene 80 mg/ml

shown in Figure 6(c), the geopolymers paving block particles display a relatively dense morphology, yet some empty spaces remain on the surface of the geopolymer composite. This could be due to the graphene agglomeration phenomenon, where the graphene distribution is less homogeneous, resulting in ineffective filling of the voids in the geopolymer composite (Saafi et al., 2015). Excessive graphene addition or poor dispersion can cause agglomeration due to van der Waals forces between graphene sheets, which affects the distribution of graphene particles within the geopolymer composite (Ranjbar et al., 2015; Saafi et al., 2015). TEM analysis confirms the successful incorporation and distribution of graphene in the geopolymer composite matrix.

## CONCLUSIONS

Fly ash-based geopolymer paving block composites have been successfully synthesized with the addition of low-cost graphene (LSE-G) additives using a natural curing system. The addition of LSE-G to the geopolymer paving block composite resulted in significant changes in the Raman spectra, indicating the successful distribution of LSE-G in the geopolymer matrix. The peak shifts in the Raman spectra suggest interactions between LSE-G and the geopolymer matrix, as well as changes in the structure and defect distribution of the material as the LSE-G concentration increases. The addition of LSE-G up to a concentration of 40 mg/ml in the geopolymer composite increased compressive strength by 21.83 MPa (a 23.4% increase) and surface hardness by 122.5 Hv (a 6.15% increase). However, at higher concentrations (80 mg/ml), a decrease in compressive strength by around 3.2% and hardness by approximately 0.33% was observed due to LSE-G agglomeration, which reduced the homogeneous distribution within the composite matrix. The addition of LSE-G reduced water absorption by 10.71% at a concentration of 40 mg/ml. However, at 80 mg/ml, water absorption slightly increased by around 2.96% due to the non-uniform distribution of LSE-G caused by agglomeration. SEM analysis displayed a denser and more compact morphology of the geopolymer composite, with a maximum reduction in porosity of 26.80% at the addition of 40 mg/ml LSE-G, owing to the graphene nanotechnology filling the voids/pores. However, increasing the LSE-G concentration

(80 mg/ml) led to a slight increase in porosity of about 17.11%. EDX analysis confirmed the presence of carbon (C) in the geopolymer composite with LSE-G addition, indicating the homogenization of LSE-G in the composite matrix. TEM analysis revealed that the addition of LSE-G could increase material density and compactness by filling the voids/pores. However, at high concentrations (80 mg/ml), LSE-G agglomeration could disrupt the uniform distribution within the matrix, making it less effective in reducing porosity. The addition of LSE-G to the geopolymer composite showed interactions between LSE-G and the geopolymer matrix, which only affected the FTIR peak intensity without altering the geopolymer structure.

## Acknowledgment

This work was supported by the Ministry of Education, Culture, Research, and Technology Republic of Indonesia via the Riset Terapan scheme (contract number: 20687/UN19.5.1.3/AL.04/2024).

## REFERENCES

1. Abiodun, O., Kabubo, C., Mutuku, R., & Ejowomu, O. (2023). The effect of pristine graphene on the mechanical properties of geopolymer mortar. *Sustainability*, 15(2), 1706. <https://doi.org/10.3390/su15021706>
2. Ahmad, M., & Rashid, K. (2022). Novel approach to synthesize clay-based geopolymer brick: Optimizing molding pressure and precursors' proportioning. *Construction and Building Materials*, 322, 126472. <https://doi.org/10.1016/j.conbuildmat.2022.126472>
3. Amran, Y. H. M., Alyousef, R., Alabduljabbar, H., & El-Zeadani, M. (2020). Clean production and properties of geopolymer concrete; A review. *Journal of Cleaner Production*, 251, 119679. <https://doi.org/10.1016/j.jclepro.2019.119679>
4. Amri, A., Amartya, A., Ilham, Y., Sutikno, S., Reni Yenti, S., Ibrahim, B., Heltina, D., Mondinos, N., Altarawneh, M., & Jiang, Z.-T. (2023). The addition of low-cost few layers graphene (FLG) to improve flexural strength of coal fly ash based-geopolymer. *Journal of Materials Research and Technology*, 24, 8849–8855. <https://doi.org/10.1016/j.jmrt.2023.05.150>
5. Amri, A., Fathurrahman, G., Najib, A. A., Awaltanova, E., Aman, & Chairul. (2018). Composites of palm oil fuel ash (POFA) based geopolymer



- and graphene oxide: structural and compressive strength. *IOP Conference Series: Materials Science and Engineering*, 420, 012063. <https://doi.org/10.1088/1757-899X/420/1/012063>
6. Amri, A., Hendri, Y. B., Zultiniar, Malindo, E., & Rahman, M. M. (2019). Graphene nanosheets (GNs) addition on the palm oil fuel ash (POFA) based geopolymer with KOH activator. *Journal of Physics: Conference Series*, 1351(1), 012101. <https://doi.org/10.1088/1742-6596/1351/1/012101>
7. Amri, A., Kurniawan, R., Sutikno, S., Yenti, S. R., Rahman, M. M., & Hendri, Y. B. (2020). Compressive strength of coal fly-ash based geopolymer with integration of graphene nanosheets (GNs). *Journal of Physics: Conference Series*, 1655(1), 012005. <https://doi.org/10.1088/1742-6596/1655/1/012005>
8. Bai, Y., Guo, W., Wang, J., Xu, Z., Wang, S., Zhao, Q., & Zhou, J. (2022). Geopolymer bricks prepared by MSWI fly ash and other solid wastes: Moulding pressure and curing method optimisation. *Chemosphere*, 307, 135987. <https://doi.org/10.1016/j.chemosphere.2022.135987>
9. Bellum, R. R., Muniraj, K., Indukuri, C. S. R., & Madduru, S. R. C. (2020). Investigation on performance enhancement of fly ash-GGBFS based graphene geopolymer concrete. *Journal of Building Engineering*, 32, 101659. <https://doi.org/10.1016/j.jobe.2020.101659>
10. Beniamin, A. M. H. A., Mohamed, N. H. N., & Yusof, M. (2023). The effect of graphene nanoplatelets content on the hardness of Mg6%Zn0.2%Mn composites. *Pertanika Journal of Science and Technology*, 31(3), 1493–1502. <https://doi.org/10.47836/pjst.31.3.20>
11. Chairunnisa, N., Triandika June, R., Nurwidayati, R., & Yuniati Pratiwi, A. (2024). The influence of curing treatments on compressive strength and durability of geopolymer paving blocks. *E3S Web of Conferences*, 476, 01036. <https://doi.org/10.1051/e3sconf/202447601036>
12. Chintalapudi, K., & Pannem, R. M. R. (2020). An intense review on the performance of Graphene Oxide and reduced Graphene Oxide in an admixed cement system. *Construction and Building Materials*, 259, 120598. <https://doi.org/10.1016/j.conbuildmat.2020.120598>
13. Chu, H., Zhang, Y., Wang, F., Feng, T., Wang, L., & Wang, D. (2020). Effect of graphene oxide on mechanical properties and durability of ultra-high-performance concrete prepared from recycled sand. *Nanomaterials*, 10(9), 1718. <https://doi.org/10.3390/nano10091718>
14. Cremonuzzi, J. M. de O., Pinto, G. M., Mincheva, R., Andrade, R. J. E., Raquez, J.-M., & Fehine, G. J. M. (2023). The micromechanics of graphene oxide and molybdenum disulfide in thermoplastic nanocomposites and the impact to the polymer-filler interphase. *Composites Science and Technology*, 243, 110236. <https://doi.org/10.1016/j.compscitech.2023.110236>
15. Dabhi, S. D., & Jha, P. K. (2017). Tuning of electronic properties and dynamical stability of graphene oxide with different functional groups. *Physica E: Low-Dimensional Systems and Nanostructures*, 93, 332–338. <https://doi.org/10.1016/j.physe.2017.07.002>
16. Dalal, S. P., & Dalal, P. (2021). Experimental investigation on strength and durability of graphene nanoengineered concrete. *Construction and Building Materials*, 276, 122236. <https://doi.org/10.1016/j.conbuildmat.2020.122236>
17. Danial, N. S., Che Halin, D. S., Ramli, M. M., Abdulllah, M. M. A., Mohd Salleh, M. A. A., Mat Isa, S. S., Talip, L. F. A., & Mazlan, N. S. (2019). Graphene geopolymer hybrid: A review on mechanical properties and piezoelectric effect. *IOP Conference Series: Materials Science and Engineering*, 572(1), 012038. <https://doi.org/10.1088/1757-899X/572/1/012038>
18. Do, Q. M., Ngo, P. M., & Nguyen, H. T. (2020). Characteristics of a fly ash-based geopolymer cured in microwave oven. *Key Engineering Materials*, 850, 63–69. <https://doi.org/10.4028/www.scientific.net/KEM.850.63>
19. Dovbeshko, G., Fesenko, O., Dementjev, A., Karpicz, R., Fedorov, V., & Posudievsky, O. Y. (2014). Coherent anti-stokes Raman scattering enhancement of thymine adsorbed on graphene oxide. *Nanoscale Research Letters*, 9(1), 263. <https://doi.org/10.1186/1556-276X-9-263>
20. Eckmann, A., Felten, A., Verzhbitskiy, I., Davey, R., & Casiraghi, C. (2013). Raman study on defective graphene: Effect of the excitation energy, type, and amount of defects. *Physical Review B*, 88(3), 035426. <https://doi.org/10.1103/PhysRevB.88.035426>
21. Fan, J., Li, M., Duan, P., Chen, W., & Zhang, Z. (2023). Sulfate attack resistance of graphene oxide reinforced geopolymer. *Cailiao Daobao/Materials Reports*, 37(13), 22030196.
22. Fiset, J., Cellier, M., & Vuillaume, P. Y. (2020). Macroporous geopolymers designed for facile polymers post-infusion. *Cement and Concrete Composites*, 110, 103591. <https://doi.org/10.1016/j.cemconcomp.2020.103591>
23. Guerrieri, M., Sanjayan, J., & Mohd Ali, A. Z. (2020). *Geopolymer damage due to leaching when exposed to water* (pp. 74–78). [https://doi.org/10.1007/978-3-030-43332-1\\_15](https://doi.org/10.1007/978-3-030-43332-1_15)
24. Guo, G., Lv, C., Liu, J., & Wang, L. (2022). Properties of fiber-reinforced one-part geopolymers: A review. *Polymers*, 14(16), 3333. <https://doi.org/10.3390/polym14163333>
25. Hu, J., Ma, J., Wang, L., & Huang, H. (2014). Preparation of La<sub>1-x</sub>Sr<sub>x</sub>MnO<sub>3</sub>/graphene thin

- films and their photocatalytic activity. *Materials Science and Engineering: B*, 180, 46–53. <https://doi.org/10.1016/j.mseb.2013.11.005>
26. Jelic, I., Savic, A., Milojcic, T., Sljivic-Ivanovic, M., Dimovic, S., Jankovic, M., Perovic, I., Zakic, D., & Antonijevic, D. (2023). Development of low carbon and energy-efficient geopolymer-based paving blocks. *Science of Sintering*, 00, 59–59. <https://doi.org/10.2298/SOS231009059J>
  27. Jonbi, J., & Fulazzaky, M. A. (2020). Modeling the water absorption and compressive strength of geopolymer paving block: An empirical approach. *Measurement*, 158, 107695. <https://doi.org/10.1016/j.measurement.2020.107695>
  28. Kaftelen-Odabaşı, H. (2024). Evaluation of morphological, structural, thermal, electrical, and chemical composition properties of graphene oxide, and reduced graphene oxide obtained by sequential reduction methods. *Carbon Trends*, 17, 100429. <https://doi.org/10.1016/j.cartre.2024.100429>
  29. Kavipriya, S. (2022). Geopolymer concrete paver blocks: A review. *Materials Research Proceedings*, 284–289. <https://doi.org/10.21741/9781644901953-32>
  30. Kosor, T., Nakić-Alfirević, B., & Gajović, A. (2016). Geopolymerization index of fly ash geopolymers. *Vibrational Spectroscopy*, 85, 104–111. <https://doi.org/10.1016/j.vibspec.2016.04.005>
  31. Lee, S., Van Riessen, A., & Chon, C.-M. (2016). Benefits of sealed-curing on compressive strength of fly ash-based geopolymers. *Materials*, 9(7), 598. <https://doi.org/10.3390/ma9070598>
  32. Merino-Lechuga, A. M., Lamaa, G., Silva, R. V., de Brito, J., Jiménez, J. R., Fernández-Rodríguez, J. M., & González-Caro, Á. (2024). Accelerated carbonation of alkali-activated vibro-compacted pervious concrete paving blocks. *Construction and Building Materials*, 449, 138458. <https://doi.org/10.1016/j.conbuildmat.2024.138458>
  33. Ni, Z., Wang, Y., Yu, T., & Shen, Z. (2008). Raman spectroscopy and imaging of graphene. *Nano Research*, 1(4), 273–291. <https://doi.org/10.1007/s12274-008-8036-1>
  34. No, Y.-S., Choi, H. K., Kim, J.-S., Kim, H., Yu, Y.-J., Choi, C.-G., & Choi, J. S. (2018). Layer number identification of CVD-grown multilayer graphene using Si peak analysis. *Scientific Reports*, 8(1), 571. <https://doi.org/10.1038/s41598-017-19084-1>
  35. Pandey, S. P., Yu, H., Lau, C., & Ng, K. (2024). New and sustainable coal char-based paving blocks for roadway applications. *Buildings*, 14(5), 1275. <https://doi.org/10.3390/buildings14051275>
  36. Papanai, G. S., Sharma, I., & Gupta, B. K. (2020). Probing number of layers and quality assessment of mechanically exfoliated graphene via Raman fingerprint. *Materials Today Communications*, 22, 100795. <https://doi.org/10.1016/j.mtcomm.2019.100795>
  37. Ranjbar, N., Mehrli, M., Mehrli, M., Alengaram, U. J., & Jumaat, M. Z. (2015). Graphene nanoplatelet-fly ash based geopolymer composites. *Cement and Concrete Research*, 76, 222–231. <https://doi.org/10.1016/j.cemconres.2015.06.003>
  38. Rao, R., Podila, R., Tsuchikawa, R., Katoch, J., Tishler, D., Rao, A. M., & Ishigami, M. (2011). Effects of layer stacking on the combination Raman modes in graphene. *ACS Nano*, 5(3), 1594–1599. <https://doi.org/10.1021/nn1031017>
  39. Saafi, M., Tang, L., Fung, J., Rahman, M., & Ligat, J. (2015). Enhanced properties of graphene/fly ash geopolymeric composite cement. *Cement and Concrete Research*, 67, 292–299. <https://doi.org/10.1016/j.cemconres.2014.08.011>
  40. Salman, S. D., Jubier, N. J., & Alzubaidi, A. B. (2023). Geopolymer concrete production by using binder nano bauxite. *Journal of Ecological Engineering*, 24(10), 305–314. <https://doi.org/10.12911/22998993/169182>
  41. Shamsaei, E., de Souza, F. B., Yao, X., Benhelal, E., Akbari, A., & Duan, W. (2018). Graphene-based nanosheets for stronger and more durable concrete: A review. *Construction and Building Materials*, 183, 642–660. <https://doi.org/10.1016/j.conbuildmat.2018.06.201>
  42. Singh, N. (2018). Fly ash-based geopolymer binder: A future construction material. *Minerals*, 8(7), 299. <https://doi.org/10.3390/min8070299>
  43. Subaer, Ekaputri, J. J., Fansuri, H., & Abdullah, M. A. B. (2017). *The relationship between Vickers microhardness and compressive strength of functional surface geopolymers*. 020170. <https://doi.org/10.1063/1.5002364>
  44. Sukmak, P., Horpibulsuk, S., & Shen, S.-L. (2013). Strength development in clay-fly ash geopolymer. *Construction and Building Materials*, 40, 566–574. <https://doi.org/10.1016/j.conbuildmat.2012.11.015>
  45. Susanto, A., Haris, A., & Saleh, M. (2024). The effect of graphene oxide (GO) on mechanical properties of fly ash-based geopolymer-GO composites. *Advances in Science and Technology*, 141, 63–68. <https://doi.org/10.4028/p-Y2vRw7>
  46. Uma Magesvari, M., Muthaiyan, P., Yugasini, S., & Ammaippan, M. (2020). Experimental studies on pervious geopolymer concrete. *IOP Conference Series: Materials Science and Engineering*, 989(1), 012032. <https://doi.org/10.1088/1757-899X/989/1/012032>
  47. Varrla, E., Paton, K. R., Backes, C., Harvey, A., Smith, R. J., McCauley, J., & Coleman, J. N. (2014). Turbulence-assisted shear exfoliation of graphene using household detergent and a kitchen blender. *Nanoscale*, 6(20), 11810–11819. <https://doi.org/10.1039/c4nr03560g>

48. Wang, Q., Ran, K., Ding, Z. Y., & Qiu, L. G. (2012). Research on mechanical properties of geopolymer concrete under early stage curing system. *Applied Mechanics and Materials*, 164, 492–496. <https://doi.org/10.4028/www.scientific.net/AMM.164.492>
49. Yan, S., He, P., Jia, D., Yang, Z., Duan, X., Wang, S., & Zhou, Y. (2016). Effects of treatment temperature on the reduction of GO under alkaline solution during the preparation of graphene/geopolymer composites. *Ceramics International*, 42(16), 18181–18188. <https://doi.org/10.1016/j.ceramint.2016.08.134>
50. Zainal, F. F., Hussin, K., Rahmat, A., Abdullah, M. M. A. B., & Shamsudin, S. R. (2016). *A study on hardness behavior of geopolymer paste in different condition*. 040001. <https://doi.org/10.1063/1.4958762>
51. Zerfu, K., & Ekaputri, J. J. (2016). Review on alkali-activated fly ash based geopolymer concrete. *Materials Science Forum*, 841, 162–169. <https://doi.org/10.4028/www.scientific.net/MSF.841.162>
52. Zhang, B., Yuan, P., Guo, H., Deng, L., Li, Y., Li, L., Wang, Q., & Liu, D. (2021). Effect of curing conditions on the microstructure and mechanical performance of geopolymers derived from nano-sized tubular halloysite. *Construction and Building Materials*, 268, 121186. <https://doi.org/10.1016/j.conbuildmat.2020.121186>
53. Zhang, G., & Lu, J. (2018). Experimental research on the mechanical properties of graphene geopolymer. *AIP Advances*, 8(6). <https://doi.org/10.1063/1.5020547>
54. Zhang, L. W., Kai, M. F., & Chen, X. H. (2020). Si-doped graphene in geopolymer: Its interfacial chemical bonding, structure evolution and ultra-strong reinforcing ability. *Cement and Concrete Composites*, 109, 103522. <https://doi.org/10.1016/j.cemconcomp.2020.103522>
55. Zhang, Z., Jin, H., Wu, C., & Ji, J. (2018). Efficient production of high-quality few-layer graphene using a simple hydrodynamic-assisted exfoliation method. *Nanoscale Research Letters*, 13, 1–8. <https://doi.org/10.1186/s11671-018-2830-9>
56. Zhong, J.-H., Liu, J.-Y., Li, Q., Li, M.-G., Zeng, Z.-C., Hu, S., Wu, D.-Y., Cai, W., & Ren, B. (2013). Interfacial capacitance of graphene: Correlated differential capacitance and in situ electrochemical Raman spectroscopy study. *Electrochimica Acta*, 110, 754–761. <https://doi.org/10.1016/j.electacta.2013.04.004>